IOP Conf. Series: Materials Science and Engineering **280** (2017) 012018 doi:10.1088/1757-899X/280/1/012018

4D Biofabrication of Branching Multicellular Structures: A Morphogenesis Simulation Based on Turing's Reaction-Diffusion Dynamics

Xiaolu Zhu[1,2*] and Hao Yang[1]

[1]College of Mechanical and Electrical Engineering, Hohai University, Changzhou, Jiangsu 213022, China
[2]Changzhou Key Laboratory of digital Manufacture Technology, Hohai University, Changzhou, Jiangsu 213022, China

*Correspondence should be addressed to: Xiaolu Zhu (zhuxiaolu@hhu.edu.cn)

Abstract. The recently emerged four-dimensional (4D) biofabrication technique aims to create dynamic three-dimensional (3D) biological structures that can transform their shapes or functionalities with time when an external stimulus is imposed or when cell postprinting self-assembly occurs. The evolution of 3D pattern of branching geometry via self-assembly of cells is critical for 4D biofabrication of artificial organs or tissues with branched geometry. However, it is still unclear that how the formation and evolution of these branching pattern are biologically encoded. We study the 4D fabrication of lung branching structures utilizing a simulation model on the reaction-diffusion mechanism, which is established using partial differential equations of four variables, describing the reaction and diffusion process of morphogens with time during the development process of lung branching. The simulation results present the forming process of 3D branching pattern, and also interpret the behaviors of side branching and tip splitting as the stalk growing, through 3D visualization of numerical simulation.

1. Introduction

One of the main objectives of three-dimensional (3D) printing in health science is to mimic biological functions [1-3]; however, it is hard to control the shape and functions of the printed 3D bio-construct/materials after being printed because of the reorganization of the printed bio-construct via cellular self-organization. Thus, regulation the transformation or functionalities of 3D biological structures with time is critical for achieving the 3D bio-construct with expected shape and functions [4, 5]. To reach this goal, a four-dimensional (4D) biofabrication technique might be utilized, which aims to create dynamic 3D biological structures that can transform their shapes or functionalities with time when an external stimulus is imposed or when cell postprinting self-assembly occurs[6]. The evolution of 3D pattern with branching geometry via self-assembly of cells is critical for 4D biofabrication of artificial organs or tissues with branched geometry.

Recent research on organ morphogenesis has described an elaborate pattern of branching phenomena [7, 8]. In the lung, two primary forms of branching have been identified: side branching and tip splitting. The branching occur in sequence: first, side branching creates the primary stalks; then, there is a change of mode to tip splitting. The kidney developmental program encodes the intricate branching and organization of approximately 1 million functional units (nephrons)[9]. These

phenomena have been hypothesized to be under genetic controls [7, 10, 11]. Since how genes could possibly act to produce these patterns is still not clear, the coding for branch patterning is possibly simplified by repeated use of a branching mechanism, as in Mandelbrot's fractal model and other elegant algorithms[12-15].

The reaction – diffusion (RD) model based on Turing-type mechanism has shown its potential power on simulating the dynamic process of molecules and tissue morphogenesis [16-18] with time. This is a suitable method to guide the 4D biofabrication via predicting the dynamic evolution of 3D self-organized microstructures. The RD model commonly involves a morphogen pair [19] (an activator- inhibitor pair) in which the inhibitor diffuse more rapidly than its activator. In recent study of lung branching morphogenesis based on reaction-diffusion model [20, 21], a four variable partial differential equation (PDE), due to Meinhardt[22], was utilized to describe the reaction and diffusion of morphogens creating branched lung development. Usually, the bone morphogenetic protein-4 (BMP4) can serves as activator, the matrix gamma-carboxyglutamic acid protein (MGP) can serve as inhibitor, and substrate S can be fibroblast growth factor 10 (FGF10). Here, we attempt to simulate the phenomena as the stalk growing, side branching and tip splitting by using a 3D branching model based on RD-based dynamics. The branching morphogenesis both in longitudinal (growth) direction and the transverse direction of the stalk is simulatively demonstrated.

2. Mathematical model

The mathematical model based on Turing's reaction-diffusion (RD) dynamics, due to Meinhardt[22], involves concentrations of activator, inhibitor, substrate and cell differentiation marker four variables. Here, the four variables are labeled as A, H, S and Y and the mathematical expressions are as follows:

$$\begin{cases} \dfrac{\partial A}{\partial t} = \dfrac{cA^2S}{H} - \mu A + D_A\nabla^2 A + \rho_A Y & (1) \\ \dfrac{\partial H}{\partial t} = cA^2S - \nu H + D_H\nabla^2 H + \rho_H Y & (2) \\ \dfrac{\partial S}{\partial t} = c_0 - \gamma S - \varepsilon YS + D_S\nabla^2 S & (3) \\ \dfrac{\partial Y}{\partial t} = dA - eY + \dfrac{Y^2}{1+fY^2} & (4) \end{cases}$$

The model postulates four spatially continuous variables, each of which is a spatio-temporal function. A, H, S, and Y are four concentration variables indicating concentrations of activator, inhibitor, substrate and cell differentiation marker. In the model, μ, ν, γ and e represent the first-order degradation rate of A, H, S and Y respectively; D_A, D_H and D_S are the diffusion coefficient of activator, inhibitor and substrate; Differentiated Y cells secrete activator A and inhibitor H at the rates of ρ_A and ρ_H respectively; c is the positive rate of activator A in the autocatalytic reaction; c0 and ε are the production and consumption rates of Substrate S. cA^2S/H describes the autocatalytic generation of activator A under the interaction of substrate S and inhibitor H; cA^2S describes the generation of inhibitor H under the interaction of activator A and substrate S; dA describes cell differentiation marker generated by activator A; $D_A\nabla^2A$, $D_H\nabla^2H$ and $D_S\nabla^2S$ describe the diffusion of activator, inhibitor and substrate respectively. High concentrations of activator A produces cell commitment Y (the dA term in the equation (4)). When the concentration of activator A exceeds a certain critical value, cell differentiation (Y = 1 indicates that cells have been differentiated) is irreversibly activated (the sigmoidal term $Y^2/(1+fY^2)$ in the equation (4)). Here, all physical quantities are dimensionless. The mathematical model was solved by the finite difference method in the MATLAB platform and the parameters were traversed in a certain range, which was also implemented for solving other RD models[23, 24]. Three-dimensional data were displayed by 3D visual software (Voxler, trail version).

The simulation run on a computer with an 8-core CPU and at least 16G of memory. Usually one set of parameters needs about several hours to twenty hours.

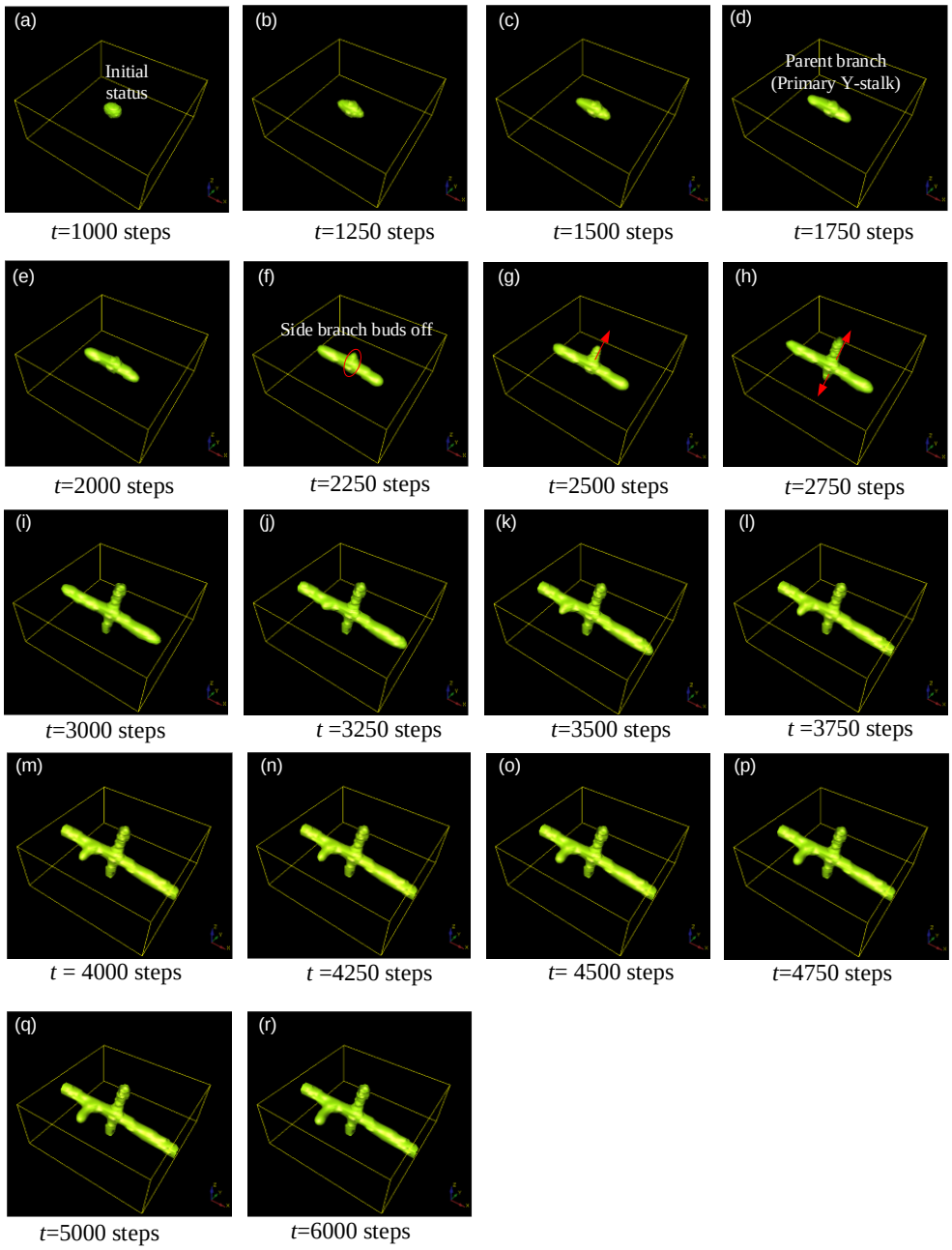

Figure 1. Simulation results for side-branching behaviors in 3D. The presented structure is the spatial distribution of the cellular differentiation marker Y. The number under image denotes the step number in simulation. Parameters: $c = 0.04$, $\mu = 0.3$, $v = 0.03$, $\rho_A = 0.03$, $\rho_H = 0.0001$, $c_0 = 0.02$, $\gamma = 0.02$, $\varepsilon = 0.042$, $d = 0.008$, $e = 0.1$, $f = 10$, $D_A = 0.1$, $D_H = 0.26$, $D_S = 0.06$.

3. The evolution of side branching

Lung development begins with side branches emerging in rows around the circumference of the parent/primary branch. The parent branch elongates and new side branches bud off in the typical domain branching. In this model, the primary branch (*Y*-stalk) grows through the positive feedback of

the peaks of activator. Also, inhibitor *H* is produced is proportional to the activator distribution and H diffuses from high-concentration region to low-concentration region. The stalk elongates because the *H* that diffuses to the side of the primary branch serves as lateral inhibition which results in vimineous elongation of the *Y* stalk rather than isotropic expansion as shown in Figure 1. The elongation of activator peak continues to generate the differentiated cells *Y* in the local region. Thus, the elongated primary branch has been formed as shown in Figure 1a-d. However, *Y* cells consume *S* (the - εYS term in the equation (3)), and S concentration becomes lower at the location of Y-stalk, but relatively higher away from the Y-stalk. Therefore, the gradient of S forms, which is the main driver of activator migration because the activator A is always seeking the substrate S according to the term $+cA^2S/H$ in equation (1). Consequently, the newly formed activator peak will migrate in the direction from low *S* concentration to high *S* concentration as indicated by the arrows in Figure1g and h (the arrow directions are away from the present stalk). Along the direction perpendicular to the primary stalk, side branches emerge when the attraction of the substrate overcomes the inhibition (Figure 1 f-r). Each activator peak in 3D on the *Y*-stalk leads to a side branch as that activator peak migrates into regions of high-concentration *S* far away from the main *Y*-stalk, where *Y* cells have depleted *S*.

4. Tip bifurcation

In this simulation, the dynamic process leading to tip bifurcation begins with the lateral extending of activator A concentration profile. Since substrate S in the current position is exhausted, the activator no longer moves in the former direction and has to look for new substrate S perpendicularly to the former stalk extension direction. The specific dynamic process is shown in Figure 2.

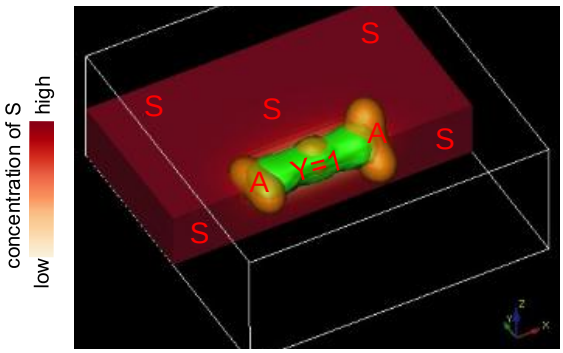

Figure 2. Schematic illustration of the profile of activator concentration along the direction transverse to stalk elongation.

There are two lateral extending behaviors of activator A concentration profiles in the horizontal and vertical planes respectively (figure 2). The white border represents the boundary of simulation domain; the red rectangle represents substrate S and substrate S distributes throughout the simulation domain space. Here only about 1/4 is taken for description and the deeper the color, the higher the substrate S concentration. The green part represents the differentiated cells (Y = 1). The orange ellipsoid indicates the isosurface of activator A. It can be seen from Fig. 1, concentration of substrate S is low around the differentiated cells (the term $-\varepsilon YS$ in equation (3) leads to the local concentration decrease of substrate S), whereas activator A extends to high concentration of substrate S direction (the term cA^2S/H in eq. (1) leads to large value of A in the region of high S). High concentration of substrate S exists in the domain perpendicular to original direction, which results in transversal expanding of activator A. And then concentration of activator A shows a flat long profile.

In order to study the distribution and relative time-dependent changes of activator A and inhibitor H in the transverse direction perpendicular to the stalk extension, the typical bifurcation (tip splitting) was simulated. Here, we select the simulation results of 2800, 3150 and 3600 steps and draw the corresponding 3D graphics of multicellular morphology for numerical analysis. Specific numerical

values and variation tendency of activator A and inhibitor H along a certain spatial coordinate axis *k* are vividly shown in figure 3.

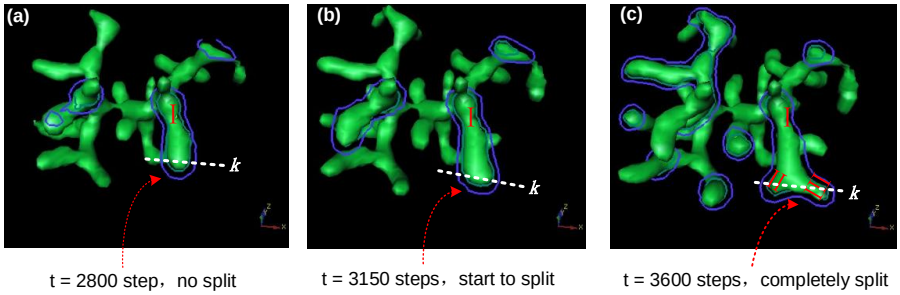

Figure 3. Simulation results for branching behaviors in the typical tip bifurcation. (a-c) Spatial distribution of the cellular differentiation marker Y; The tip bifurcation could be examined along the spatial axis *k* on the plane defined by the blue closed contours. Parameters: c=0.04, μ=0.8, ν=0.08, ρ_A=0.03, ρ_H=0.0001, c_0=0.02, γ=0.02, ε=0.042, d=0.008, e=0.1, f=10, D_A=0.1, D_H=0.26, D_S=0.06.

Figure 3 shows the dynamic process of tip bifurcation and concentration distribution relationships between activator A and inhibitor H. Figure 3a, b, c show 3D graphics of cell differentiation marker Y isosurface. Stalk I extends longitudinally along the original direction (figure 3a, steps 2800); Tip of stalk I becomes large and flat indicating the tip expands, perpendicularly, transverse to original direction (figure 3b, steps 3150); Tip of stalk I completely splits and stalk I is divided into two daughter branches, namely branch II and branch III (figure 3c, steps 3600). The symmetrical center plane of stalk I serves as tangent plane (the plane defined by blue and green contours, figure 3a, b, c). A line with the largest width through the tip of stalk I is made on the tangent plane (denoted by the blue closed contour) , which is denoted by *k* (the white dotted line, figure 3a, b, c). The concentration distribution change of inhibitor H lags behind that of activator A. The delayed inhibitor peak resembles a knife forcing the activator peak with lateral expansion into two (the inhibitor peak significantly reduces the concentration of activator at the corresponding region). After the tip splits completely, the inhibitor peak also divides into two peaks, and its distribution along the spatial axis *k* is almost the same as that of activator A (steps 3600). Further research work for the 4D biofabrication may rely on the 3D culture techniques [3, 24, 25] that are essentially constructing and regulating the dynamic structures composed of numeral cells.

5. Conclusion

Based on the Turing reaction-diffusion mechanism, the 3D simulation of the mathematical model describing bifurcation phenomena in biology, including concentrations of activator, inhibitor, substrate and cell differentiation marker were studied. This 3D simulation model can predict following patterns of 3D tissue morphology: side branches and tip bifurcation, and is able to demonstrate the evolution of side branching and tip bifurcation of the 3D multicellular structure. It lays a foundation for guiding 4D biofabrication of lung airway grafts via 3D cellular self-organization, which is expected to greatly reduce the complexity of future experimental research and number of trials.

Acknowledgments

This research was supported by grants from the National Natural Science Foundation of China (Grant No. 51505127), Natural Science Foundation of Jiangsu Province (Grant No. BK20161197), Changzhou Sci&Tech Program (Grant No. CE20165029), and the Fundamental Research Funds for the Central Universities of China (Grant No. 2015B04414).

References

[1] Chia H N and Wu B M. 2015 *Journal of Biological Engineering.* **9**: 4.

[2] Zhu X, Gojgini S, Chen T-H, Teng F, Fei P, Dong S, Segura T, and Ho C-M. 2016 *Biomedicine & Pharmacotherapy* **83**: 1203-1211.
[3] Zhu X, Gojgini S, Chen T-H, Fei P, Dong S, Ho C-M, and Segura T. 2017 *Journal of Biological Engineering* **11**(1): 12.
[4] Gao B, Yang Q, Zhao X, Jin G, Ma Y, and Xu F. 2016 *Trends in biotechnology* **34**(9): 746-756.
[5] Datta P, Ayan B, and Ozbolat I T. 2017 *Acta Biomaterialia*: doi: 10.1016/j.actbio.2017.01.035.
[6] Li Y C, Zhang Y S, Akpek A, Shin S R, and Khademhosseini A. 2017 *Biofabrication* **9**(1): 012001.
[7] Metzger R J, Klein O D, Martin G R, and Krasnow M A. 2008 *Nature* **453**(7196): 745-U1.
[8] Tzou D, Spurlin J W, Pavlovich A L, Stewart C R, Gleghorn J P, and Nelson C M. 2016 *Evodevo* **7**.
[9] Sampogna R V, Schneider L, and Al-Awqati Q. 2015 *Journal of the American Society of Nephrology* **26**(10): 2414-2422.
[10] Zhang Y, Yokoyama S, Herriges J C, Zhang Z, Young R E, Verheyden J M, and Sun X. 2016 *Proceedings of the National Academy of Sciences of the United States of America* **113**(27): 7557-7562.
[11] Morrisey E E and Hogan B L M. 2010 *Developmental Cell* **18**(1): 8-23.
[12] Mandelbrot B B, *The Fractal Geometry of Nature* [M]. 1983, New York: Freeman.
[13] Kitaoka H, Takaki R, and Suki B. 1999 *Journal of Applied Physiology* **87**(6): 2207-2217.
[14] Tebockhorst S, Lee D, Wexler A S, and Oldham M J. 2007 *Journal of Applied Physiology* **102**(1): 294-305.
[15] Kitaoka H, *Three-Dimensional Model of the Human Airway Tree Based on a Fractal Branching Algorithm*, in *Fractals in Biology and Medicine* [M], G.A. Losa, et al., Editors. 2002, Birkhäuser Basel: Basel. p. 39-46.
[16] Kondo S and Miura T. 2010 *Science* **329**(5999): 1616-1620.
[17] Menshykau D and Iber D. 2013 *Physical Biology* **10**(4): 046003.
[18] Menshykau D, Blanc P, Unal E, Sapin V, and Iber D. 2014 *Development* **141**(23): 4526-4536.
[19] Chen T H, Zhu X, Pan L, Zeng X, Garfinkel A, Tintut Y, Demer L L, Zhao X, and Ho C M. 2012 *Biomaterials* **33**(35): 9019-9026.
[20] Guo Y N, Sun M Z, Garfinkel A, and Zhao X. 2014 *Plos One* **9**(7).
[21] Guo Y N, Chen T H, Zeng X J, Warburton D, Bostrom K I, Ho C M, Zhao X, and Garfinkel A. 2014 *Journal of Physiology-London* **592**(2): 313-324.
[22] Meinhardt H. 1976 *Differentiation* **6**(2): 117-23.
[23] Zhu X and Yang H. In-Silico Constructing Three-Dimensional Hollow Structure via Self-Organization of Vascular Mesenchymal Cells [C]. in *The 16th International Conference on Nanotechnology (IEEE NANO 2016)*. 2016. Sendai, Japan: IEEE.
[24] Zhu X and Yang Y. Simulation for tubular and spherical structure formation via self-organization of vascular mesenchymal cells in three dimensions [C]. in *Image and Signal Processing, BioMedical Engineering and Informatics (CISP-BMEI), International Congress on*. 2016. IEEE.
[25] Zhu X L and Ding X T. 2017 *Slas Discovery* **22**(5): 626-634.